T. X. Cai

P. Y. Zhang

Key Laboratory of Education Ministry for Modern Design and Rotor-Bearing System, School of Mechanical Engineering, Xi'an Jiaotong University, Xi'an 710049, P.R.C.

D. F. Diao[1]

Key Laboratory of Education Ministry for Modern Design and Rotor-Bearing System, School of Mechanical Engineering, Xi'an Jiaotong University, Xi'an 710049, P.R.C.; Nanosurface Science and Engineering Research Institute, College of Mechatronics and Control Engineering, Shenzhen University, Shenzhen, 518060, P.R.C.
e-mail: dfdiao@mail.xjtu.edu.cn

Evolution of Maximum Contact Stresses in Amorphous Carbon Coated Silicon During Sliding Wear Against Si_3N_4 Ball

The evolution of the maximum contact stresses in amorphous carbon coated silicon during sliding wear against a Si_3N_4 ball was investigated. Amorphous carbon coating was prepared on a silicon substrate by the electron cyclotron resonance (ECR) plasma sputtering method. Surface morphologies of the coating and counterpart were measured by an atomic force microscope (AFM). The friction and wear behavior of the coating was studied by a ball-on-disk tribometer. The cross-sections of the wear tracks at different wear stages were observed with a scanning electron microscope (SEM). Maximum contact stresses with different coating thicknesses were calculated by the three-dimensional semi-analytical method (SAM). The results demonstrated that when taking surface asperities into consideration, maximum shear stress at the bonding interface and adjacent substrate showed a dramatic increase during wear and should be responsible for the initiation and propagation of the cracks observed at the final stage of sliding. [DOI: 10.1115/1.4023409]

Keywords: maximum contact stress, coating thickness, amorphous carbon, sliding wear, SAM

1 Introduction

Amorphous carbon coatings, one of the most intensively researched and widely applied thin films, show extraordinary tribological property and wear resistance in fields such as microelectromechanical systems (MEMS), high-density magnetic recording systems, and biomechanical devices [1–3]. From the viewpoint of designing amorphous carbon coatings, it is well known that the maximum contact stresses, namely, maximum tensile stress, maximum shear stress, and maximum von Mises stress play important roles in engineering applications because the wear regime and fracture mechanism of the coatings are mainly determined by these maximum stresses [4–6].

During sliding wear, the change in coating thickness holds the key to the wear because it gradually alters the maximum contact stresses. There are many published studies focused on the friction and wear behaviors of amorphous carbon coatings with respect to coating thickness. Wang and Kato [7,8] studied the coating thickness dependence of initial wear of nitrogen-doped amorphous carbon sliding against a diamond tip, and the results indicated that both the critical load and critical number of friction cycles for observable wear particles generation increased with increasing coating thickness. Dorner et al. [9] studied the abrasive wear resistance of diamond-like carbon (DLC) coated Ti_6Al_4V with a variety of coating thicknesses, and they found that the cohesive failure of the DLC is dependent on the coating thickness. Bai et al. [10] evaluated the scratch wear resistance of super thin carbon nitride overcoat by an AFM with a diamond tip. Observation of the scratched grooves indicated that the wear mechanism for a coating thickness less than 5 nm was brittle fracture in substrate and abrasive wear; the wear modes transformed to plow and plastic deformation when overcoat thickness was 6–10 nm. Therefore, clarifying the evolution of maximum contact stresses induced by thickness change during sliding wear is important for control of wear behavior.

There are many published studies on the contact stresses distributions of coating under sliding contact by numerical or analytical methods. O' Sullivan and King [11] analyzed three-dimensional quasi-static stress states by employing the least-squares approach and determined the distributions of von Mises stresses in the coating and substrate. Komvopoulos [12,13] studied the elastic contact problem of a coated semi-infinite solid compressed by a rigid surface with the finite element method (FEM). Michler and Blank studied the failure mechanisms of the substrate and coating composite [14] through a parametric elastic-plastic finite element analysis (FEA) for the common load case of the indentation of spherical bodies into a layered surface considering a wide range of coating thicknesses. Roman and Gabriel [15] proposed a simplified algorithm for solving the contact problem of elasticity connected with an indentation of a rigid sphere in an elastic half-space [16] covered by an elastic layer, and they studied the ratio between maximal tensile stress and von Mises stress on the surface of the heterogeneous half-space and at the layer-half-space interface at different parameters. A number of researchers have also applied the boundary element method (BEM) [17,18] to analyze wear cracks numerically in layered elastic solids. The semi-analytical method is an alternative way to solve the contact problems. The conjugate gradient method (CGM) [19,20] and the fast Fourier transform technique (FFT) [21] are widely applied to calculate the contact pressure on layered elastic solid. Chen et al. [22] developed a fast SAM model for solving the three-dimensional elastoplastic contact problems involving layered materials using the equivalent inclusion method (EIM). On the other hand, Diao et al. [23,24] introduced the local yield map and interface yield map of a hard coating under sliding contact, showing the yielding position by evaluating the critical maximum contact pressures for yielding at the different positions using the FEM method. Recently, Zhang et al. [25] studied the three-dimensional local yield initiation of the coated substrate system in the contact region of a ball on disk model by SAM. The studies mentioned above provided valuable knowledge about the contact stresses of an ideal flat coating sliding against a surface with a certain radius.

[1]Corresponding author.

Contributed by the Tribology Division of ASME for publication in the JOURNAL OF TRIBOLOGY. Manuscript received July 8, 2012; final manuscript received December 16, 2012; published online March 18, 2013. Assoc. Editor: Dong Zhu.

However, solid surfaces contain irregularities or deviations from a prescribed geometrical form [26]. The contact modeling of two rough surfaces is of considerable meaning in the study of friction and wear [27–29]. Many studies have been reported on the contact mechanics analysis of rough surfaces. Cai and Bhushan [30] investigated the contact behavior of rough, multilayered elastic-perfectly plastic solid surfaces with a numerical three-dimensional contact model. Dini and Hills [31] studied the interfacial contact pressure and shear traction distributions for a sphere pressed onto an elastically similar half-space whose surface is populated by a uniform array of spherical asperities. Students and Rudzitis [32] examined stresses under the elliptical Hertzian contact area, which appear during a real contact between two asperities in the process of sliding friction. However, few studies has been carried out on the evolving maximum contact stresses of amorphous carbon coating with thickness changing in a realistic ball-on-disk tribosystem.

This paper, therefore, concentrates on the evolution of maximum contact stresses in amorphous carbon coating during sliding wear against a Si_3N_4 ball from the viewpoint of realistic industrial applications. For this purpose, an amorphous carbon coating was prepared on a silicon substrate with an electron cyclotron resonance plasma sputtering system. Surface asperities of the coating and counterpart Si_3N_4 ball were measured with an atomic force microscope. Friction coefficient and wear life of the coating were measured with a ball-on-disk (BOD) tribometer. Coating thickness and cross-sectional views of the coating during wear were obtained by post-sliding scanning electron microscope observation. According to the experimental results, contact models were solved to analyze the stresses in the coating-substrate system at different thicknesses by the semi-analytical method.

2 Experiment Details

2.1 Preparation of Carbon Coatings. Amorphous carbon coating was prepared on polished silicon substrate (p-type $\langle 100 \rangle$) by the ECR plasma sputtering method. The working schematic of the system was described in detail elsewhere [33]. Substrates were cut into 20×20 mm^2 squares and then cleaned in acetone before fixed onto the substrate holder. The background and operating pressure in the vacuum chamber were 3×10^{-6} and 3×10^{-4} Torr, respectively. The substrate holder was heated to 400 °C and the temperature was kept at 400 ± 1 °C during deposition and for one hour after the deposition. A high-purity carbon target was used as the carbon source, and argon was used as bombardment gas. Silicon substrate was in situ sputter-cleaned prior to deposition by 3 min bombardment etching with Ar^+ of 5 eV to remove any residual contaminants. A divergent magnetic field and microwave were combined to generate argon plasma before a target bias voltage was applied. Carbon atoms were, consequently, sputtered off the target, and coatings were formed on the substrate by applying a substrate bias voltage. A typical set of deposition parameters in this study is as follows: target bias voltage of −300 V, substrate bias voltage of +10 V, and deposition time of 60 min.

2.2 Characterizations of Carbon Coating and Si_3N_4 Ball. Thickness of the as-deposited carbon coating was measured by cross-sectional observation with a field emission scanning electron microscope (jt-6700F). A uniform value of 300 nm was measured. The value was also checked through step height measurement at the margin area of the prepared carbon coating and silicon substrate. By taking the deposition time of 60 min into consideration, a depositing rate of 5 nm per minute could be calculated.

Adherence of the carbon coating to the silicon substrate was examined by a triboindenter (Hysitron TI950). Nano-scratch tests were carried out on the coating with a diamond tip (radius of 100 nm) under normal load of up to 8 mN. Results showed that after 40 repeated segments the coating adheres to the substrate well, and no delamination was observed from the substrate.

Surface roughness of the carbon coating and Si_3N_4 ball (used as counterpart in the following tribotest) was measured by an atomic force microscope (Innova), and the roughness images were fixed to 20×20 μm^2 scan size and 256×256 sample data size to minimize scale-related roughness variations. Figure 1 shows the isometric views of the as-deposited carbon coating and the Si_3N_4 ball surface as measured by the AFM with the no contact mode. It can be seen that both surfaces possess finite roughness with microscopic asperity features. According to Greenwood and Williamson [34] (GW), the roughness of two approaching surfaces could be combined into an infinitely smooth surface and a surface with spherically shaped asperities having a uniform mean radius r and following a Gaussian height distribution. Table 1 summarizes the individual and combined GW roughness parameters [35] extracted from the AFM topographical data of the coating and Si_3N_4 ball. σ is the standard deviation of surface heights, r is the mean radius of curvature of asperity, and η is the areal density of asperities. The standard deviation of the asperity heights of the combined surfaces could be computed as $\sigma^2 = {\sigma_1}^2 + {\sigma_2}^2$, while for the combined values of r and η, they follow the relationships that $1/r^2 = 1/{r_1}^2 + 1/{r_2}^2$ and $({r_1}^2 + {r_2}^2)/\eta = {r_2}^2/\eta_1 + {r_1}^2/\eta_2$, respectively. In this study, $\sigma \times r \times \eta = 0.036$, also noting from Archard [36] that $\sigma \times r \times \eta = constant$ (0.03–0.05).

2.3 Ball-On-Disk Tribotest and Post-Sliding Observation. A ball-on-disk type tribometer was used for cyclic sliding tests on an amorphous carbon coating. A detailed schematic diagram of the apparatus could be found in a former published study [33]. The test samples were fixed onto the sample holder, which is driven by a ball spindle with rotary accuracy of 2 μm. The Si_3N_4

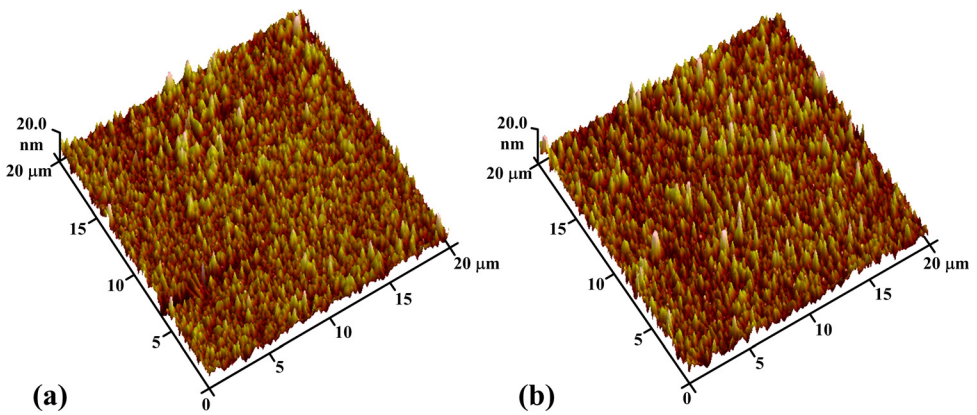

Fig. 1 AFM topographical images of (*a*) Si_3N_4 ball surface and (*b*) carbon coating surface measured at 20×20 μm^2

Table 1 Individual and combined GW Roughness parameters

	Individual surfaces		Combined surface
Roughness parameters	Ball	Coating	Ball/coating
σ/nm	4.04	4.14	5.785
r/μm	3.954	11.050	2.912
$\eta/\mu m^{-2}$	2.1375	2.1325	2.1366

ball was fixed at the end of the cantilever as the counterpart. Normal load of 1 N was applied on the pallet after a balance of the cantilever was gained by adjusting the balance weight. During the test, the disk was rotated at a constant speed of 180 rpm, and the decentration between the contact center and the rotary spindle was 1.4 mm. The signal of friction force was collected with the strain gauge pasted on the cantilever with an accuracy of 0.02 N. All experiments were performed in ambient conditions (20–25 °C, 40–60% RH). It should be noted that plenty of tribotests were carried out under the same experiment parameters, it was found that all test specimens have similar wear lives, and the reproducibility of the tribological experiment is good.

Mean depths of the wear track at the carbon coating surface were measured with a white light interferometry (WLI) (Taylor Hobson CCI 6000) after certain cycles of sliding wear. The CCI 6000 system was used for fast three-dimensional profilometry with z-axis resolution of 0.1 nm. The scan size was set as 1×1 mm^2, and the sample data size was set as 256×256. Mean wear depths values were extracted by measuring surface profiles in the radial direction of circular wear tracks. The wear volumes at each step of friction test were calculated with area of wear track cross-sections. Specific wear rate was calculated according to the volume of the material loss as a function of sliding distance. The cross-sections of the wear tracks after different sliding cycles were examined by an SEM.

3 Experiment Results

3.1 Tribological Properties of Amorphous Carbon Coating. Figure 2 shows the friction coefficients and the mean wear depths of the as-deposited amorphous coating sliding against a Si_3N_4 ball. It can be seen that after a short period of running-in, the friction coefficient decreases to a relatively low value of 0.090 rapidly and stabilizes at a mean value of 0.122 for about 20,000 sliding cycles. Meanwhile, the mean depth of the wear track gradually increases during sliding, the values of which are 15.5 nm for 1500 cycles, 92.5 nm for 7500 cycles, and 217.5 nm for 18,750 cycles, respectively. The specific wear rate of the coating was calculated by measuring the volume of the material loss after certain sliding distance, and the value is 1.216×10^{-6} mm^3/(N · m). It should be

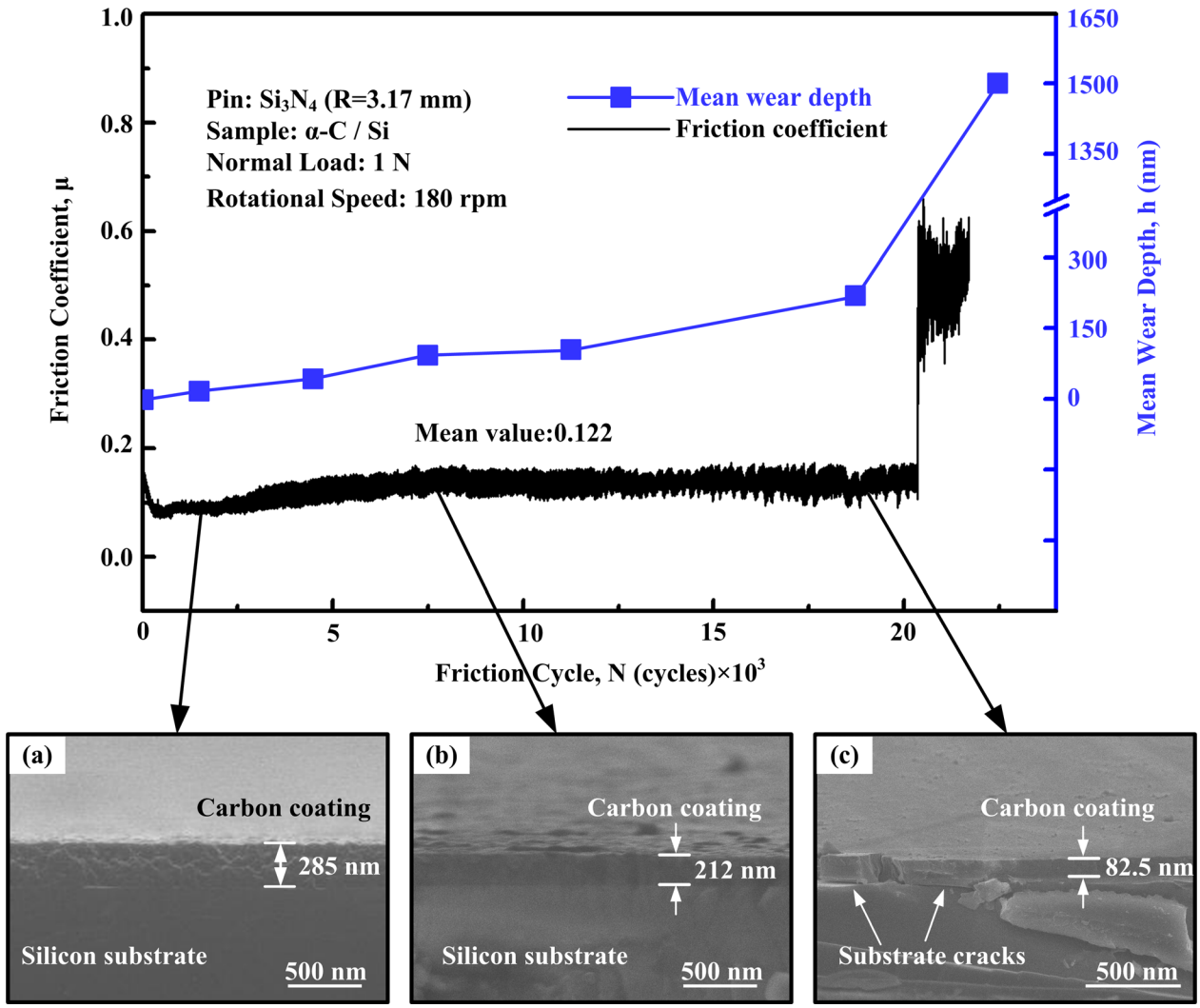

Fig. 2 Friction coefficients and mean wear depths of carbon coating during sliding wear against a Si_3N_4 ball. Insets are post-sliding SEM observations on cross-sections of the wear tracks of (*a*) 1500 cycles, (*b*) 7500 cycles, and (*c*) 18,500 cycles, respectively.

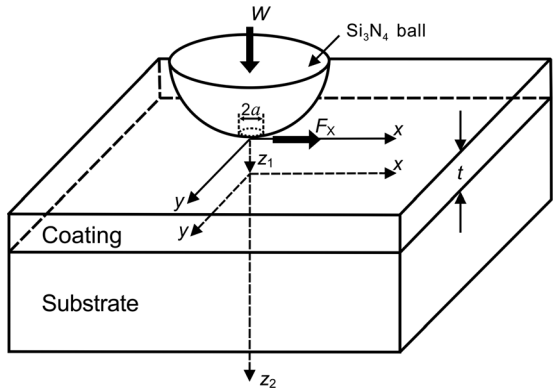

Fig. 3 3D SAM contact model of Si_3N_4 ball and amorphous carbon coated substrate during sliding wear

noted that after a long period of steady sliding wear, the friction coefficient dramatically increases to 0.506 at the sliding cycle of 20,355 cycles of wear, which marks the fracture of the entire coating. Furthermore, since wear rate change corresponds to the wear mode change [37], a rapid increase in the mean wear depth is observed due to high wear rate caused by severe wear of the unprotected silicon substrate.

Figures 2(*a*)–2(*c*) show the edge-on SEM images of wear tracks taken after 1500, 7500, and 18,500 sliding cycles, respectively. For coatings at an early stage after 1500 cycles of sliding wear, the coating thickness was 285 nm as shown in Fig. 2(*a*). The cross-section SEM image of the center of the wear track shows that no plastic deformation was found at the bonding interface or in the substrate along the cross-section of the wear track. For coatings at middle stage of wear after 7500 cycles, the thickness of the coating was decreased uniformly to 212 nm, and a clear and undamaged interface could be observed at this stage as shown in Fig. 2(*b*). For coatings at final stage after 18,500 cycles, thickness of the coating is 82.5 nm as shown in Fig. 2(*c*). Moreover, cracks were found in the silicon substrate and were fairly closed to the bonding interface. Noting that soon after this period in the wear test, fragmentation of the entire carbon coating was observed after 20,355 sliding cycles. It should be pointed out that the loading condition was uniform at each friction point during tribotests. And we viewed many cross-sections and checked the coating thicknesses at different cross-sections along the same wear track; the cross-sections at each friction step are similar, and values of thicknesses were in accordance with those shown in Fig. 2 as well. The wear measurements correspond to the average of the SEM images randomly taken on the wear track. Also, no crack was observed until the coating thickness reached the critical value of 82.5 nm. The propagation and connection of the substrate cracks at the final stage was believed to be the reason of delamination of bulk coating material, and the wear mechanism thus could be adhesive failure at the end of sliding wear.

4 Contact Stresses Analysis

4.1 3D SAM Method. Figure 3 shows a three-dimensional ball-on-disk contact model of the Si_3N_4 ball and an amorphous carbon coated silicon substrate. The coating is assumed to be of a uniform thickness t and is perfectly bonded to an elastic substrate. Normal load W and tangential forces F_x are both applied on the top of the Si_3N_4 ball. a refers to the actual radius of the contact zone. The coordinate is proposed, in which the surface of the coating and the bonding interface are defined as $z_1 = 0$ and $z_2 = 0$ ($z_1 = t$), respectively.

Table 2 Calculation parameters

Parameters	Value
Load, W (N)	1
Friction coefficient, μ	0.122
Tangential load, F_x(N)	μW
Ball radius, R (mm)	3.17
Young's modulus of ball, E_1 (GPa)	336.9
Young's modulus of coating, E_c (GPa)	142.3 [33]
Young's modulus of substrate, E_b (GPa)	131.0
Possion's ratio of ball, ν_1	0.22
Possion's ratio of coating, ν_c	0.30
Possion's ratio of substrate, ν_b	0.28
Hardness of the coating, H_c (GPa)	14.09 [33]
Hardness of the substrate, H_b (GPa)	13.0
Maximum Hertzian pressure, P_{max} (MPa)	609.3202
Hertzian contact radius, a_0 (μm)	27.98
Thickness of coating, t (μm)	(0.05, 0.10, 0.15, 0.20, 0.25, 0.30, 0.40, 0.50, 0.60, 0.70, 0.75, 0.80, 0.90, 1.00, 1.50) × a_0

The calculation parameters are given in Table 2. Normal load W was fixed at 1 N. Tangential load F_x was determined by the friction coefficient measured in the experiment, where μ was equal to 0.122 obtained from the experiment results. P_{max} and a_0 are the maximum Hertzian contact pressure and Hertzian contact radius with uncoated condition, correspondingly. It should be noted that in the following results, the stresses were normalized by P_{max}, and the coordinates were normalized by a_0.

For the boundary conditions, only the shear traction in the x direction q_x is involved while the frequency response functions, corresponding to the traction q_y, can be obtained from symmetrical characters along the $y = 0$ plane. The applied loads consists of normal pressure $p(x,y)$ and shear traction $q_x(x,y)$. The boundary conditions at the upper layer surface ($z_1 = 0$) are given by

$$\sigma_{zz}^{(1)}(x,y,0) = -p(x,y), \quad \sigma_{xz}^{(1)}(x,y,0) = q_x(x,y), \quad \sigma_{yz}^{(1)}(x,y,0) = 0 \tag{1}$$

The continuous conditions for the stresses and displacements at the interface between the coating and substrate are as follows:

$$\begin{aligned} &\sigma_{xz}^{(1)}(x,y,t) = \sigma_{xz}^{(2)}(x,y,0), \quad \sigma_{yz}^{(1)}(x,y,t) = \sigma_{yz}^{(2)}(x,y,0), \\ &\sigma_{zz}^{(1)}(x,y,t) = \sigma_{zz}^{(2)}(x,y,0), \\ &u_x^{(1)}(x,y,t) = u_x^{(2)}(x,y,0), \quad u_y^{(1)}(x,y,t) = u_y^{(2)}(x,y,0), \\ &u_z^{(1)}(x,y,t) = u_z^{(2)}(x,y,0) \end{aligned} \tag{2}$$

In the substrate, the stresses and displacements should vanish at a large distance from the contact surface:

$$\sigma^{(2)}(x,y,\infty) = 0, \quad u^{(2)}(x,y,\infty) = 0 \tag{3}$$

In this contact model, surface displacements, subsurface normal stresses (σ_{xx}, σ_{yy},σ_{zz}), and subsurface shear stresses (σ_{xy}, σ_{yz}, σ_{zx}) distributions were calculated by using the three-dimensional semi-analytical method, in which conjugate gradient method and discrete convolution and fast Fourier transform (DC-FFT) technique were used for higher solution speed. A detailed description of the numerical method was reported in Refs. [25,38]. Then the von Mises stress σ_{vm} in the contact zone was calculated with the normal stresses and shear stresses, where σ_{vm} was defined as follows

$$\sigma_{vm} = \frac{1}{\sqrt{2}}\sqrt{(\sigma_{xx}-\sigma_{yy})^2 + (\sigma_{yy}-\sigma_{zz})^2 + (\sigma_{zz}-\sigma_{xx})^2 + 6(\sigma_{xy}^2 + \sigma_{yz}^2 + \sigma_{zx}^2)} \tag{4}$$

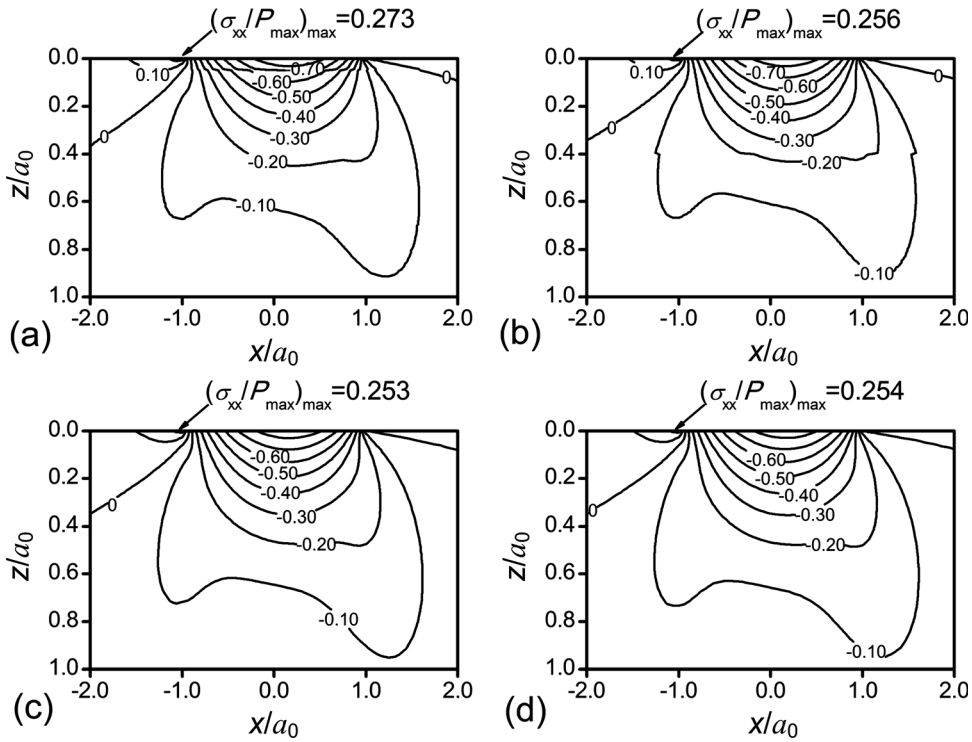

Fig. 4 Contour plots of the normalized tensile stress in the $y = 0$ plane for $E_c/E_b = 1.086$ and $\mu = 0.122$; (*a*) $t = 0.05a_0$, (*b*) $t = 0.40a_0$, (*c*) $t = a_0$, (*d*) $t = 1.50a_0$

4.2 3D SAM Contact Stresses Results. Contours of the three normalized contact stresses, namely normal stress σ_{xx}, shear stress $\sigma_{zx,}$ and von Mises stress σ_{vm}, in the $y = 0$ plane, calculated from the sliding contact model with different normalized coating thickness from 0.05 to 1.50 are shown in Figs. 4–6, respectively. The values of stresses in the figures are for the case of the friction coefficient $\mu = 0.122$ and $E_c/E_b = 1.086$, where E_c is the elastic modulus of carbon coating and E_b of silicon substrate. Accuracy of the computation has been examined by comparing with the results in the O'Sullivan and King study [11], and a difference of less than 1% was obtained (see Ref. [25]).

Figure 4 shows the distribution of normal stress σ_{xx} normalized by the maximum Hertzian contact pressure P_{max} on the diagram of x/a_0 and z/a_0 in the $y = 0$ plane. Positive values of σ_{xx}/P_{max} stands for tension, and negative values represent compression. It can be seen that the distributions of σ_{xx}/P_{max} are quite similar at four thicknesses of carbon coating, despite the sharp bending observed at the interface in Figs. 4(*a*) and 4(*b*). The maximum tensile stress always occurs at the surface of the coating. For $t = 0.05a_0$ in Fig. 4(*a*), $(\sigma_{xx}/P_{max})_{max} = 0.273$; for the cases of $t = 0.40a_0$, a_0 and $1.50a_0$ in Figs. 4(*b*)–4(*d*), the values of $(\sigma_{xx}/P_{max})_{max}$ are 0.256, 0.253, and 0.254, respectively.

For shear stress σ_{zx} distributed in the concerned plane, the normalized results are shown in Fig. 5. Two poles of the stress contours with different sign of values are observed for each case of four coating thicknesses. The sign of the stress values corresponds to the defined coordinates but make no difference in the effect of shear on the materials. In Fig. 5(*a*) for $t = 0.05a_0$, the regions of high absolute value of σ_{zx}/P_{max} occur in the silicon substrate, where the maximum value of $|\sigma_{zx}/P_{max}|$ is 0.245. In Fig. 5(*b*) for $t = 0.40a_0$, the regions of high values of $|\sigma_{zx}/P_{max}|$ are observed in the substrate and around the bonding interface, where $|\sigma_{zx}/P_{max}|_{max} = 0.255$ is generated at the bonding interface. When coating thicknesses are a_0 and $1.50a_0$ in Figs. 5(*c*) and 5(*d*), the maximum values of σ_{zx} both occur in the coating, where $|(\sigma_{zx}/P_{max})|_{max} = 0.256$ in Fig. 5(*c*) and $|(\sigma_{zx}/P_{max})|_{max} = 0.255$ in Fig. 5(*d*).

Figure 6 shows the contour plots of the dimensionless von Mises stress. In Fig. 6(*a*) for $t = 0.05a_0$, the regions of high value of σ_{vm}/P_{max} occur in the substrate, where the maximum value of σ_{vm}/P_{max} is 0.371. In Fig. 6(*b*) for $t = 0.40a_0$, the regions of high values of σ_{vm}/P_{max} are observed in the substrate and around the bonding interface, where $(\sigma_{vm}/P_{max})_{max} = 0.383$ is generated at the bonding interface. In both Fig. 6(*c*) for $t = a_0$ and Fig. 6(*d*) for $t = 1.50a_0$, the region of highest value of σ_{vm}/P_{max} is generated in the coating, where $(\sigma_{vm}/P_{max})_{max} = 0.375$ in Fig. 6(*c*) and $(\sigma_{vm}/P_{max})_{max} = 0.377$ in Fig. 6(*d*).

Figure 7 shows the relationship between maximum values of normalized contact stresses (σ_{xx}/P_{max}, σ_{zx}/P_{max}, and σ_{vm}/P_{max}) and normalized coating thickness (t/a_0) calculated at four positions in the $y = 0$ plane. $\psi_T(x, 0, z)$is employed to represent the value of $(\sigma_{xx}/P_{max})_{max}$ and ψ_{Ts}, ψ_{Tc}, ψ_{Ti}, ψ_{Tb} are the values of $\psi_T(x, 0, z)$ at the surface, in the coating, at the interface, and in the substrate, respectively. Similarly, $\psi_S(x, 0, z)$ and $\psi_Y(x, 0, z)$ are used to represent the values of $(\sigma_{zx}/P_{max})_{max}$ and $(\sigma_{vm}/P_{max})_{max}$ in the concerned plane, respectively. For contact stresses at the surface of the coating shown in Fig. 7(*a*), maximum tensile stress ψ_T is dominant and its value generally keeps at steady level of 0.25∼0.28 as t/a_0 decreases from 1.50 to 0.05 reflecting the whole wear process. Also, the maximum values of shear stress, ψ_S and maximum von Mises stress ψ_Y at this position both hold at a stable stage for the same range of t/a_0, the values of ψ_S and ψ_Y are around 0.10 and 0.20, respectively. For contact stresses in the carbon coating shown in Fig. 7(*b*), as t/a_0 decreases from 1.50 to 0.50, ψ_T shows an overall stable trend except for some tiny fluctuations when t/a_0 is less than 0.80, ψ_S almost keeps at a constant value of 0.26, and the maximum value of the von Mises stress ψ_Y keeps at a high level around 0.37. With a further decrease of t/a_0 from 0.50 to 0.05, ψ_T increases from 0.18 to 0.27 in wave, while ψ_S and ψ_Y both show a decrease in this period. For contact stresses at the bonding interface and those in the silicon substrate shown in Figs. 7(*c*) and 7(*d*), it is obvious that ψ_T at both positions turn out to be the least dominant among the three in general, even though an obvious increase of maximum tensile stress were observed when t/a_0 is between 0.05 and 0.50, which should be due to the effect of surface traction. For the interface (see Fig. 7(*c*)), maximum shear stress ψ_S increased from 0.09 to 0.25

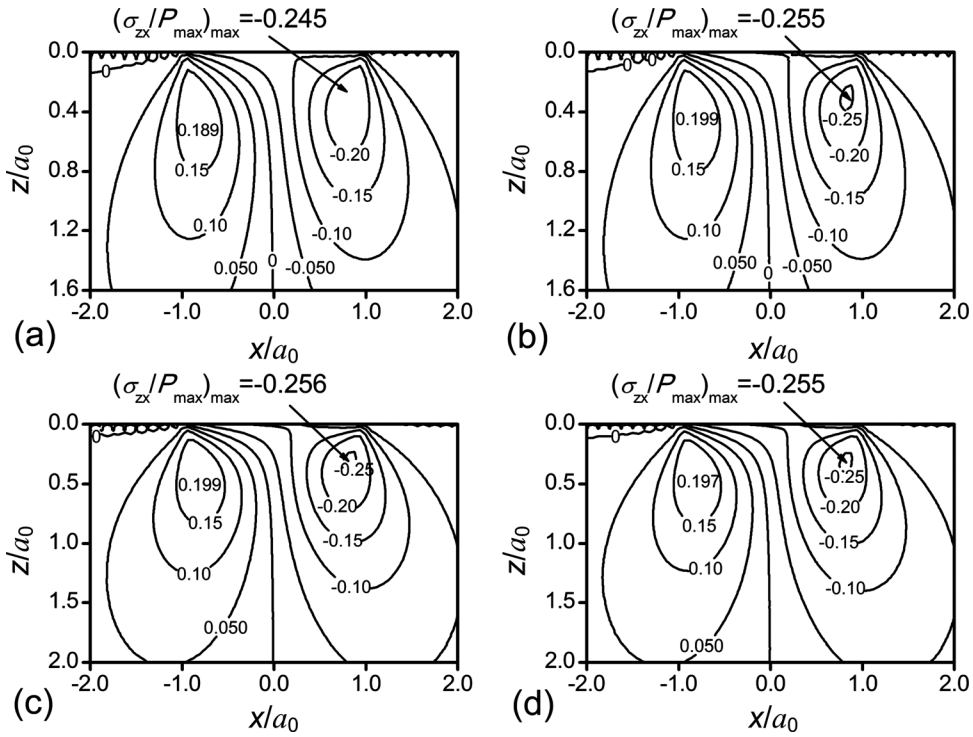

Fig. 5 Contour plots of the normalized shear stress in the $y = 0$ plane for $E_c/E_b = 1.086$ and $\mu = 0.122$; (*a*) $t = 0.05a_0$, (*b*) $t = 0.40a_0$, (*c*) $t = a_0$, (*d*) $t = 1.50a_0$

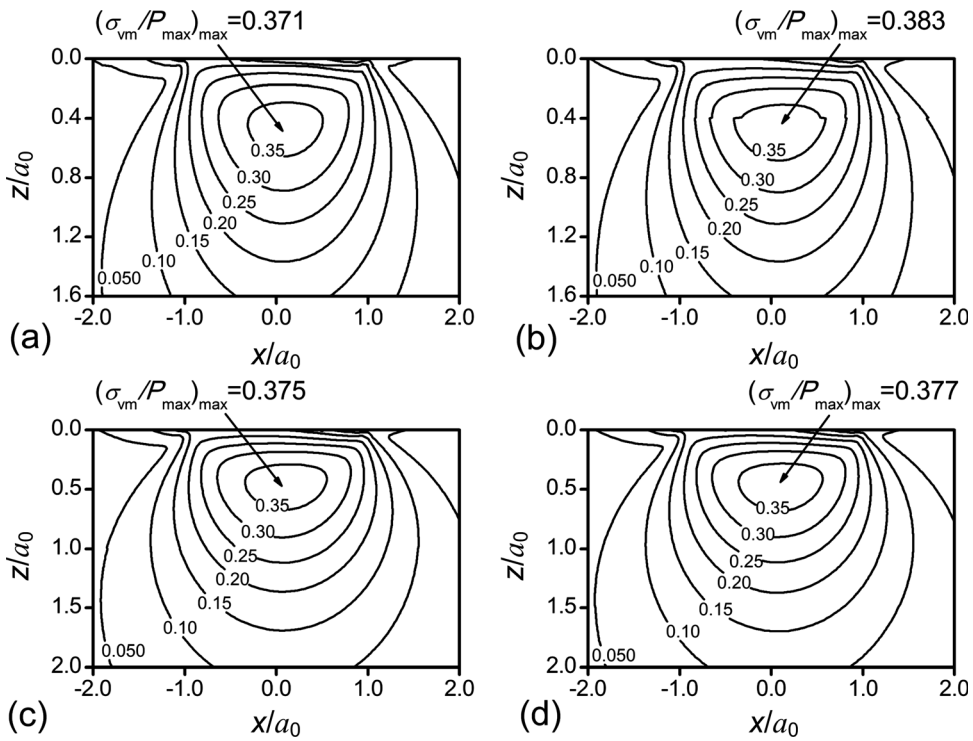

Fig. 6 Contour plots of the normalized von Mises stress in the $y = 0$ plane for $E_c/E_b = 1.086$ and $\mu = 0.122$; (*a*) $t = 0.05a_0$, (*b*) $t = 0.40a_0$, (*c*) $t = a_0$, (*d*) $t = 1.50a_0$

and maximum von Mises stress ψ_Y from 0.18 to 0.37 as t/a_0 decreased from 1.50 to 0.50, and both stresses show similar evolving trends with that in the carbon coating as t/a_0 further decreased from 0.50 to 0.05 (see Fig. 7(*b*)). For the substrate (see Fig. 7(*d*)), ψ_S increased from 0.09 to 0.25 and ψ_Y from 0.18 to 0.38 as t/a_0 decreased from 1.50 to 0.50, and both stresses hold at the high values as t/a_0 further decreased from 0.50 to 0.05. It should be noted that during sliding wear, the maximum values of shear stress and von Mises stress at the interface show a similar trend with that in the substrate when t/a_0 is larger than 0.50, while show similar trend with that in the coating when t/a_0 is smaller than 0.50. Such coherence indicates that ψ_S and ψ_Y in the substrate

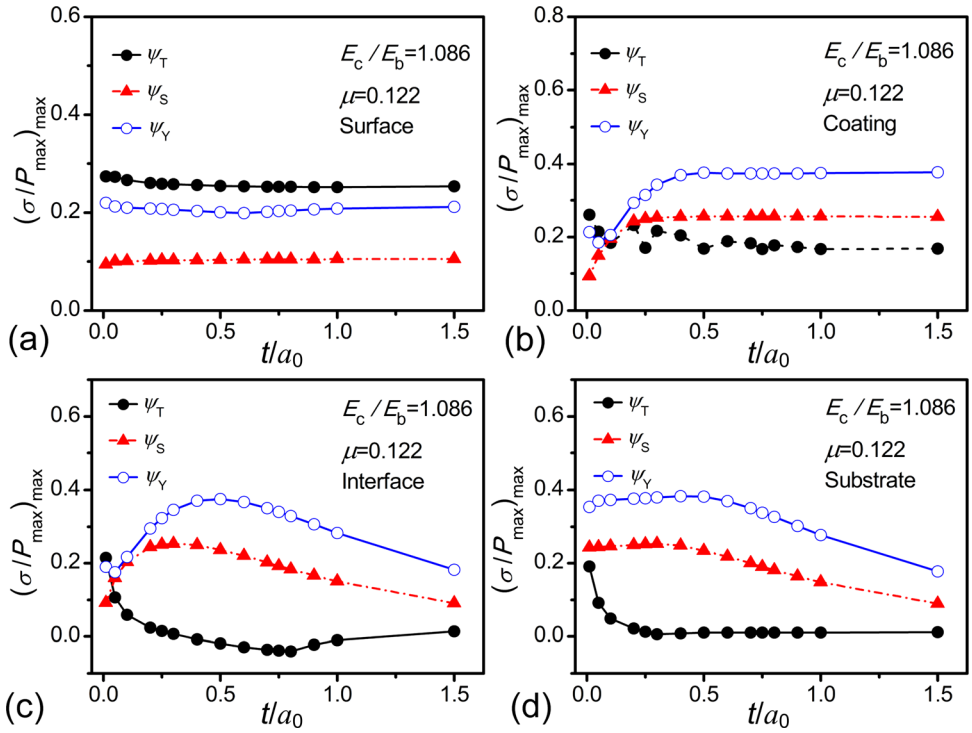

Fig. 7 Evolution of the normalized maximum contact stresses $(\sigma/P_{max})_{max}$ with t/a_0 change during sliding wear, (*a*) at the surface, (*b*) in the coating, (*c*) at the interface, (*d*) in the substrate for $E_c/E_b = 1.086$ and $\mu = 0.122$, where ψ_T, ψ_S, and ψ_Y refers to the maximum values of the normalized tensile stress (σ_{xx}/P_{max}), normalized shear stress (σ_{zx}/P_{max}) and normalized von Mises stress (σ_{vm}/P_{max}), respectively

locate close to the interface when t/a_0 is larger than 0.50, and ψ_S and ψ_Y in the coating locate close to the interface when t/a_0 is smaller than 0.50.

It is well known that shear stress at the bonding interface plays an important role in adhesive failure during sliding contact, and equivalent stress of von Mises is responsible for the initiation and propagation of microcracks induced by local plastic deformation. In order to clarify the exact reason dominating the coating failure, a very effective way is to evaluate the critical maximum contact pressure for the onset of shear or yield. Either shear or yield may occur firstly, and it is determined by a relatively lower value of the critical maximum contact pressure $P_{max,c}$. It has been mentioned in the previous studies of Diao et al. [23,24] that the critical maximum contact pressure $P_{max,Y}$ for initiation of yield could be obtained as follows:

$$P_{max,Y} = \mathrm{Min}[Y(x,0,z)/\psi_Y(x,0,z)] \tag{5}$$

Here $Y(x, 0, z)$ is the distribution of the yield strength in the $y = 0$ plane. In this study, $Y(x, 0, z)$ only relies on the value of z, when $z < t$, $Y(x, 0, z) = Y_c$, and when $z > t$, $Y(x, 0, z) = Y_b$, where Y_c and Y_b are the yield strength of the coating and substrate materials, respectively.

Similarly, the critical maximum contact pressure $P_{max,S}$ for occurrence of shear could be

$$P_{max,S} = \mathrm{Min}[-S(x,0,z)/\psi_S(x,0,z)] \tag{6}$$

Here $S(x, 0, z)$ is the distribution of the shear strength in the $y = 0$ plane. In accord with the condition of evaluation of yield initiation, $S(x, 0, z)$ relies on the value of z, when $z < t$, $S(x, 0, z) = S_c$, and when $z > t$, $S(x, 0, z) = S_b$, where S_c and S_b are the shear strength of the coating and substrate materials, respectively. The negative sign is used to eliminate the directional effect of the calculated shear stress in the defined coordinate.

Figures 8(*a*)–8(*d*) show the comparisons between the normalized critical maximum contact pressures ($P_{max,c}/H_b$) for initiation of shear ($P_{max,S}/H_b$) and that for initiation of yield ($P_{max,Y}/H_b$) with t/a_0 change at four positions in the coating-substrate system. Note that the hardness of the silicon substrate H_b is used for the normalization of both critical contact pressures. A simple assumption is made that $H_b = 3Y_b = 6S_b$ and $H_c = 3Y_c = 6S_c$, which is widely accepted in practical applications for ductile and isotropic materials. Note that the relationship was used since wear of the coating is a mild and homogeneous process (no large scale brittle fracture of coating was observed). And it is also due to the difficulties in measuring the yield strength of amorphous carbon coatings. Therefore, the values of Y_c/Y_b and S_c/S_b are both calculated as 1.084 by H_c/H_b. It could be seen that the calculated critical maximum contact pressure for occurrence of shear and yield generally reveal similar trend varying with t/a_0 at four positions. For the surface, the values of $P_{max,Y}$ and $P_{max,S}$ are almost on the same level, indicating that yield and shear could probably occur simultaneously at the coating surface (Fig. 8(*a*)). For the coating, $P_{max,Y}$ is larger than $P_{max,S}$ for a wide range of t/a_0 from 1.50 to 0.05, which means the effect of shear is dominant for fractures at this position (Fig. 8(*b*)). For the interface and substrate, which are most concerned with coating delamination in this study, shear is still dominant and generally shows stronger and stronger influence during wear. Thus, it can be concluded that during the sliding wear of carbon coated silicon substrate, shear plays a more important role in influencing the wear of materials in the coating, at the interface, as well as in the substrate.

Meanwhile, it is also of interest to investigate the probable initiation position of shear and its transition during wear. Figure 9 shows the relationship between the normalized critical maximum contact pressure $P_{max,S}/H_b$ for the shear and normalized coating thickness t/a_0. It should be pointed out that the shear will appear firstly from the position where the minimum value of $P_{max,S}/H_b$ locates. Thus, when t/a_0 is larger than 0.50, the shear will initiate

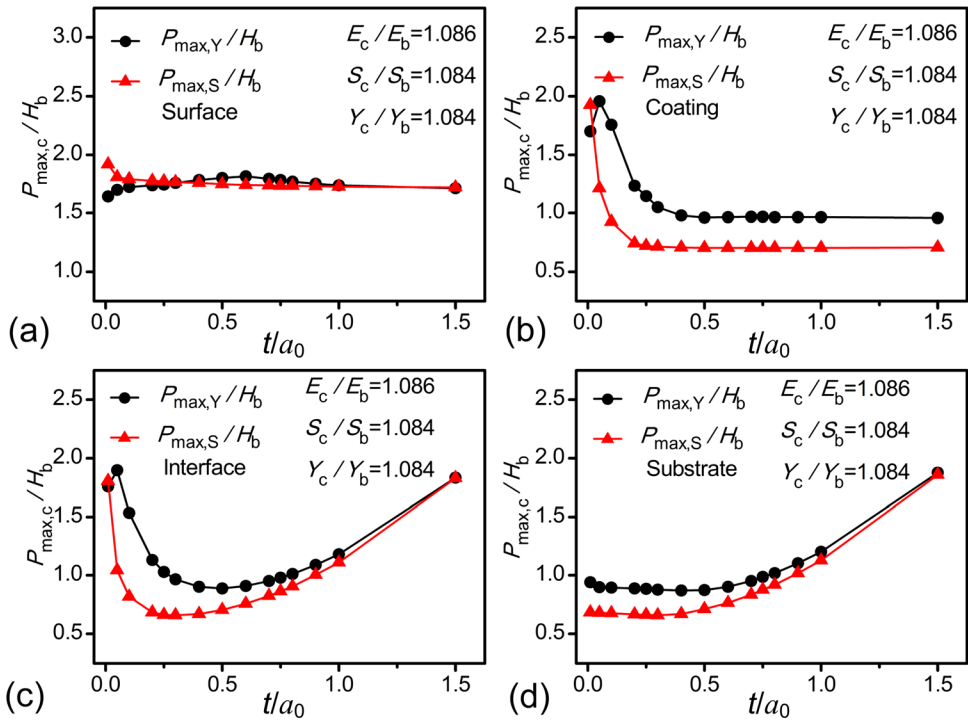

Fig. 8 Comparisons between the normalized critical maximum contact pressures ($P_{max,c}/H_b$) for initiation of shear ($P_{max,S}/H_b$) and that for initiation of yield ($P_{max,Y}/H_b$) with t/a_0 change (*a*) at the surface, (*b*) in the coating, (*c*) at the interface, (*d*) in the substrate for $E_c/E_b = 1.086$ and $\mu = 0.122$, where S_c/S_b and Y_c/Y_b are the shear strength ratio and the yield strength ratio of the coating to the substrate, respectively

in the coating while when t/a_0 gets smaller than 0.50, the shear will initiate at the bonding interface and local substrate. Based on this understanding about the transition between two states of shear initiation, one could predict the critical thickness marking the change of weak positions in a coating-substrate system.

5 Discussion

According to the computation results shown in Fig. 7, the evolution of maximum contact stresses thus could be obtained with a corresponding range of normalized coating thickness t/a_0 during sliding wear. Normally, the Hertzian contact radius a_0 was considered as the value of the Si_3N_4 ball in contact with uncoated silicon substrate. In this case, a_0 was calculated as 27.98 μm (see Table 2). As the thickness of the coating decreased from 300 nm to 82.5 nm in the sliding wear test, the range of t/a_0 was from 0.011 to 0.003, equivalently. In this instance, the coating could be regarded as ultra-thin and the distributions of the contact stresses in the coating as well as at the bonding interface were determined by stresses at the coating surface. Thus, the values of the maximum contact stresses could be considered almost invariant during the entire sliding wear process (small variation of t/a_0 in Fig. 7). It should be noted that when taking the surface asperities (see Fig. 1) into consideration, the dimensionless results of the contact stresses analysis in Figs. 4–9 are appropriate for each asperity in contact as well. While in this case, the value of a_0 used to normalize the coating thickness should be the semicontact-width of the asperities in real contact area. Because of the order of magnitudes' difference of a_0, the evolution of the maximum contact stresses due to asperity contact would be greatly different from that of the Si_3N_4 ball contact. In order to investigate the evolution of maximum contact stresses during wear in this case, the semicontact width a_0 is derived as follows:

The individual surface roughness parameters of the Si_3N_4 ball and amorphous carbon coating were obtained in the second part of this study. Corresponding combined surface roughness parameters are calculated and shown in Table 1. Greenwood and Williamson [34] have shown that the separation between the surfaces is of the order of σ to 2σ over a wide range of load; thus, the maximum interference or compression subjected to the tallest asperity will be between 2σ and 3σ, when the radius of the curvature of the asperity is r, the semicontact-width a_0 is in the range that $\sqrt{2r\sigma} < a_0 < \sqrt{3r\sigma}$, thus the value of a_0 was calculated to be between 183.6 nm and 224.8 nm. For the purpose of a simple and convenient computation, a medium value of 200 nm of a_0 was selected. Thus, the range of t/a_0 was from 1.50 to 0.40 for asperity contact during sliding wear (coating thickness between 300 nm and 82.5 nm). Note that contact mechanics are originally based on continuum mechanics that assumes uniform and continuous materials properties regardless of the scales in space and time. It is often valid when tackling scientific and engineering problems of surface interaction on a macroscale [39]. In this study, the wear performance of the coating could be mainly governed by average effects of the material properties in macroscale; thus, the dimensionless results obtained from the theoretical analysis based on the macroscale contact model are still appropriate for the multi microscale asperities contacts. And the effect of molecular or atomic level events may not be considered here. It can be seen from Fig. 7 that during sliding wear, the effect of maximum tensile stress mainly act on the coating surface. While, according to the analysis results shown in Figs. 7(*c*) and 7(*d*), the maximum shear stresses and maximum von Mises stresses at the interface and those in the adjacent substrate, namely, ψ_{Si}/ψ_{Sb} and ψ_{Yi}/ψ_{Yb}, increased by 178% and 111% during wear, correspondingly. According to Fig. 8, when t/a_0 decreased from 1.50 to 0.40, shear played the decisive role in wear of the coating at the interface as well as in the substrate. Therefore, the cracks observed in Fig. 3(*c*) are believed to be the result of repeated shear stress cycles subjected to the bonding interface and local substrate. Also, according to Fig. 9, when a_0 is equal to 200 nm, the critical value of coating thickness for shear transition is calculated as 100 nm (t/a_0 for shear transition is 0.50). Thus, once coating thickness is smaller than 100 nm due to wear, the bonding interface and local substrate

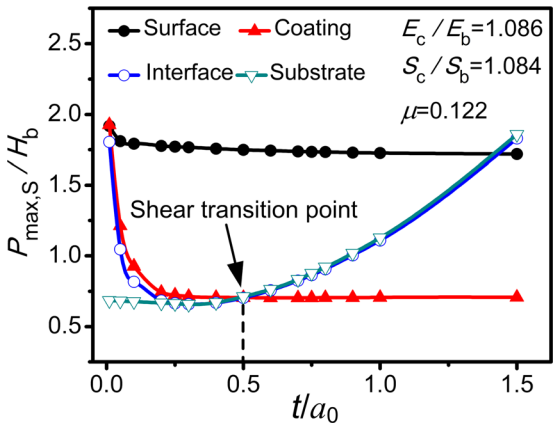

Fig. 9 Shear transition point calculated by evaluating a lower value of the normalized critical maximum contact pressure for the shear ($P_{max,S}/H_b$) at four positions with t/a_0 change during sliding wear in the coating-substrate system for $E_c/E_b = 1.086$, $S_c/S_b = 1.084$, and $\mu = 0.122$

become the most vulnerable. Therefore, the transition of shear onset position from coating to substrate could aggravate the effect of repeated shear on the local zone (including bonding interface and neighbor substrate) and is believed to play a promotive role in the initiation and propagation of cracks (Fig. 2(*c*)), probably with the pre-existence of interfacial defects. Based upon this knowledge, we could probably prevent the occurrence of interfacial cracks by presetting a safe value of coating thickness in the designing period of coated productions.

In this paper, we mainly focused on the evolutions of maximum contact stresses with one coating thickness and one set of tribological conditions, it was mainly due to the time-consuming process of tribotests. And we consider it would be better if further tests can be carried out with variations in coating thickness, friction coefficient, or combinations of coating-substrate materials. However, the defect does not obscure the conclusions drawn from the calculation and interpretation of the work. In addition, it could be deduced that the wear mode of delamination should follow the power law of low cycle fatigue proposed by Manson [40], Coffin and Schenectady [41], and Diao and Kato [42]. Therefore, the fatigue resistance of the coating could be examined with a further study upon different loading conditions, and it would be of considerable value in coating design and failure prevention as well.

6 Conclusion

The evolution of the maximum contact stresses in an amorphous carbon coated silicon substrate during sliding wear against a Si_3N_4 ball was studied by combining the experimental results and the semi-analytical method. And we proposed the method of solving the ball-on-disk contact model with realistic friction coefficient and coating thicknesses in the wear process. Discussions were made on the relationship between wear modes and maximum contact stresses based on the understanding of asperity contact. Thus, main conclusions are drawn as follows:

(1) The friction coefficient of amorphous carbon coating is 0.122, the coating thickness decreased from original 300 nm to 82.5 nm during sliding wear until bulk delamination took place. In this period, the values of maximum shear stresses and maximum von Mises stresses (ψ_{Si} and ψ_{Yi}) at the bonding interface, as well as those (ψ_{Sb} and ψ_{Yb}) in the near-interface substrate zone, increased by 178% and 111% (see Figs. 7(*c*) and 7(*d*)), correspondingly.

(2) Shear stress dominated wear in the carbon coating, at the bonding interface, as well as in the silicon substrate. Cracks observed in the substrate are initiated and propagated mainly due to repeated shear stress subjected to the bonding interface and local substrate.

(3) The normalized critical thickness for local shear transition from carbon coating to silicon substrate $t_c = 0.5a_0$, where a_0 is the semicontact-width of surface asperities. The calculated thickness of 100 nm is close to the measured value for delamination in the experiments. For the studied realistic ball-on-disk tribosystem, the method of studying the maximum contact stresses evolution based on real surfaces contact is valuable in engineering application.

Acknowledgment

The authors would like to thank the National Nature Science Foundation of China under Grant Nos. of 90923027 and 51175405 as well as the Fundamental Research Funds for Central Universities for their support.

Nomenclature

E_1 = Young's modulus of Si_3N_4 ball (GPa)
E_c = Young's modulus of amorphous carbon coating (GPa)
E_b = Young's modulus of silicon substrate (GPa)
F_x = applied tangential loads along the x direction (N)
H_b = hardness of silicon substrate (GPa)
H_c = hardness of amorphous carbon coating (GPa)
N = frictional cycle
P_{max} = maximum contact pressure (GPa)
$P_{max,c}/H_b$ = critical maximum contact pressure normalized by substrate hardness
$P_{max,S}/H_b$ = critical maximum contact pressure for the shear initiation normalized by substrate hardness
$P_{max,Y}/H_b$ = critical maximum contact pressure for the yield initiation normalized by substrate hardness
R = radius of Si_3N_4 ball (mm)
S_c = shear strength of the coating (GPa)
S_b = shear strength of the substrate (GPa)
W = normal load of tribotest (N)
Y_c = yield strength of the coating (GPa)
Y_b = yield strength of the substrate (GPa)
a = actual radius of the contact zone (μm)
a_0 = Hertzian contact radius (μm)
q_x = shear tractions along the x direction (GPa)
q_y = shear tractions along the y direction (GPa)
r = mean radius of curvature of asperity (μm)
t = coating thickness (μm)
t/a_0 = normalized coating thickness
u_x, u_y, u_z = surface displacements in x, y, and z directions (mm)
x, y, z = space coordinates (mm)
σ = standard deviation of surface asperities heights (nm)
η = areal density of asperities (μm^{-2})
μ = friction coefficient
v_1 = Poisson's ratio of Si_3N_4 ball
v_c = Poisson's ratio of amorphous carbon coating
v_b = Poisson's ratio of silicon substrate
σ_{xx} = normal stress in $y = 0$ plane (GPa)
σ_{zx} = shear stress in $y = 0$ plane (GPa)
σ_{vm} = von Mises stress in $y = 0$ plane (GPa)
ψ_T = normalized maximum tensile stress in $y = 0$ plane
ψ_S = normalized maximum shear stress in $y = 0$ plane
ψ_Y = normalized maximum von Mises stress in $y = 0$ plane

Subscripts

s, c, i, b = (in ψ_{Ti}, ψ_{Tc}, ψ_{Ti}, and ψ_{Tb}) refer to values of ψ_T at the surface, in the coating at the interface, and in the substrate, respectively; the expressions are also applied to ψ_S, ψ_Y

References

[1] Forbes, I. S., and Wilson, J. I. B., 2002, "Diamond and Hard Carbon Films for Microelectromechanical Systems (MEMS)—A Nanotribological Study," Thin Solid Films, **420**, pp. 508–514.

[2] Tsai, H. C., and Bogy, D. B., 1987, "Characterization of Diamondlike Carbon Films and Their Application as Overcoats on Thin-Film Media for Magnetic Recording," J. Vac. Sci. Technol. A, **5**, pp. 3287–3312.

[3] Erdemir, A., and Donnet, C., 2006, "Tribology of Diamond-Like Carbon Films: Recent Progress and Future Prospects," J. Phys. D: Appl. Phys., **39**, pp. R311–R327.

[4] Tangena, A. G., Wijnhoven, P. J. M., and Muijderman, E. A., 1988, "The Role of Plastic Deformation in Wear of Thin Film," ASME J. Tribol., **110**, pp. 602–608.

[5] Diao, D. F., Kato, K., and Hokkirigawa, K., 1994, "Fracture Mechanisms of Ceramic Coatings in Indentation," AMSE J. Tribol., **116**, pp. 860–869.

[6] Diao, D. F., and Kato, K., 1994, "Spalling Mechanism of Al_2O_3 Ceramic Coating Coated WC-CO Substrate under Sliding Contact," Thin Solid Films, **245**, pp. 104–108.

[7] Wang, D. F., and Kato, K., 1998, "Coating Thickness Effect on Surface Damage Mode Transitions for an Ion Beam Assisted Carbon Nitride Coating Subject to Sliding Contact With a Spherical Diamond," Wear, **223**, pp. 167–172.

[8] Wang, D. F., and Kato, K., 2003, "Coating Thickness Effects on Initial Wear of Nitrogen-Doped Amorphous Carbon in Nano-Scale Sliding Contact: Part I—In Situ Examination," Tribol. Int., **36**, pp. 649–658.

[9] Dorner, A., Schurer, C., Reisel, G., Irmer, G., Seidel, O., and Muller, E., 2001, "Diamond-Like Carbon-Coated Ti6Al4V: Influence of the Coating Thickness on the Structure and the Abrasive Wear Resistance," Wear, **249**, pp. 489–497.

[10] Bai, M. W., Kato, K., Umehara, N., Miyake, Y., Xu, J. G., and Tokisue, H., 2000, "Scratch-Wear Resistance of Nanoscale Super Thin Carbon Nitride Overcoat Evaluated by AFM With a Diamond Tip," Surf. Coat. Technol., **126**, pp. 181–194.

[11] O' Sullivan, T. C., and King, R. B., 1988, "Sliding Contact Stress Field Due to a Spherical Indenter on a Layered Elastic Half-Space," ASME J. Tribol., **109**, pp. 223–231.

[12] Komvopoulos, K., 1988, "Finite Element Analysis of a Layered Elastic Solid in Normal Contact With a Rigid Surface," ASME J. Tribol., **110**, pp. 477–485.

[13] Komvopoulos, K., 1989, "Elastic-Plastic Finite Element Analysis of Indented Layered Media," ASME J. Tribol., **111**, pp. 430–439.

[14] Michler, J., and Blank, E., 2001, "Analysis of Coating Fracture and Substrate Plasticity Induced by Spherical Indentors: Diamond and Diamond-like Carbon Layers on Steel Substrates," Thin Solid Films, **381**, pp. 119–134.

[15] Roman, K. Z., and Gabriel, R., 2010, "Stresses in Hard Coating Due to a Rigid Spherical Indenter on a Layered Elastic Half-space," Tribol. Int., **43**, pp. 1592–1601.

[16] Johnson, K. L., 1985, *Contact Mechanics*, Cambridge University Press, Cambridge, UK.

[17] Lin, W., and Keer, L. M., 1989, "Three-Dimensional Analysis of Cracks in Layered Transversely Isotropic Media," Proc. R. Soc., London, Ser. A, **424**, pp. 307–322.

[18] Kuo, C. H., and Keer, L. M., 1995, "Three-Dimensional Analysis of Cracking in a Multilayered Composite," ASME J. Appl. Mech., **62**, pp. 273–281.

[19] Nogi, T., and Kato, T., 1997, "Influence of a Hard Surface Layer on the Limit of Elastic Contact—Part I: Analysis Using a Real Surface Model," ASME J. Tribol., **119**, pp. 493–500.

[20] Polonsky, I. A., and Keer, L. M., 1999, "A Numerical Method for Solving Rough Contact Problems Based on the Multi-Level Multi-Summation and Conjugate Gradient Techniques," Wear, **231**, pp. 206–219.

[21] Liu, S. B., Wang, Q., and Liu, G., 2000, "A Versatile Method of Discrete Convolution and FFT (DC-FFT) for Contact Analyses," Wear, **243**, pp. 101–111.

[22] Chen, W. W., Zhou, K., Keer, L. M., and Wang, Q. J., 2010, "Modeling Elasto-Plastic Indentation on Layered Materials Using the Equivalent Inclusion Method," Int. J. Solids Struct., **47**, pp. 2841–2854.

[23] Diao, D. F., Kato, K., and Hayashi, K., 1992, "The Local Yield Map of Hard Coating Under Siding Contact," Proceedings of the 19th Leeds-Lyon Symposium on Tribology, Elsevier, Amsterdam, pp. 419–427.

[24] Diao, D. F., and Kato, K., 1994, "Interface Yield Map of a Hard Coating Under Sliding Contact," Thin Solid Films, **245**, pp. 115–121.

[25] Zhang, P. Y., Diao, D. F., and Wang, Z. J., 2012, "Three-Dimensional Local Yield Maps of Hard Coating Under Sliding Contact," ASME J. Tribol., **134**, p. 021301.

[26] Bhushan, B., 1998, "Contact Mechanics of Rough Surfaces in Tribology: Multiple Asperity Contact," Tribol. Lett., **4**, pp. 1–35.

[27] Bowden, F. P., and Tabor, D., 1950, *The Friction and Lubrication of Solids, Part I*, Clarendon Press, Oxford, UK.

[28] Bowden, F. P., and Tabor, D., 1964, *The Friction and Lubrication of Solids, Part II*, Clarendon Press, Oxford, UK.

[29] Bhushan, B., 1996, *Tribology and Mechanics of Magnetic Storage Devices*, Springer, New York.

[30] Cai, S. B., and Bhushan, B., 2007, "Three-Dimensional Sliding Contact Analysis of Multilayered Solids With Rough Surfaces," ASME J. Tribol., **129**, pp. 40–59.

[31] Dini, D., and Hills, D. A., 2009, "Frictional Energy Dissipation in a Rough Hertzian Contact," ASME J. Tribol., **131**, p. 021401.

[32] Students, E., and Rudzitis, J., 1996, "Contact of Surface Asperities in Wear," Tribol. Int., **29**, pp. 275–279.

[33] Fan, X., and Diao, D. F., 2011, "Contact Mechanisms of Transfer Layered Surface During Sliding Wear of Amorphous Carbon Film," ASME J. Tribol., **133**, p. 042301.

[34] Greenwood, J. A., and Williamson, J. B. P., 1966, "Contact of Nominally Flat Surfaces," Proc. R. Soc., London, Ser. A, **295**, pp. 300–319.

[35] Yu, N., and Polycarpou, A. A., 2004, "Combining and Contacting of Two Rough Surfaces With Asymmetric Distribution of Asperity Heights," ASME J. Tribol., **126**, pp. 225–232.

[36] Archard, J. F., 1953, "Contact and Rubbing of Flat Surface," J. Appl. Phys., **24**, pp. 981–988.

[37] Wang, D. F., and Kato, K., 2003, "Nano-Scale Fatigue Wear of Carbon Nitride Coatings: Part I—Wear Properties," ASME J. Tribol., **125**, pp. 430–436.

[38] Wang, Z. J., Wang, W. Z., Wang, H., Zhu, D., and Hu, Y. Z., 2010, "Partial Slip Contact Analysis on Three-Dimensional Elastic Layered Half Space," ASME J. Tribol., **132**, p. 021403.

[39] Zhu, D., and Wang, Q. J., 2012, "Elastohydrodynamic Lubrication: A Gateway to Interfacial Mechanics-Review and Prospect," ASME J. Tribol., **133**, p. 041001.

[40] Manson, S. S., 1965, "Fatigue: A Complex Subject-Some Simple Approximations," Exp. Mech., **5**, pp. 193–226.

[41] Coffin, L. F., and Schenectady, N. Y., 1954, "A Study of the Effects of Cyclic Thermal Stresses on a Ductile Metal," Trans. ASME, **76**, pp. 931–950.

[42] Diao, D. F., and Kato, K., 2012, *Wear and Wear Maps of Hard Coatings, Tribology of Polymeric Nanocomposites: Friction and Wear of Bulk Materials and Coatings*, 2nd ed., Elsevier, New York, Chap. 11.